Composites Part B 115 (2017) 117–123

Contents lists available at ScienceDirect

Composites Part B

journal homepage: www.elsevier.com/locate/compositesb

Non-linear elastic response of layered structures, alternating pentamode lattices and confinement plates

A. Amendola [a, *], G. Benzoni [b], F. Fraternali [a]

[a] Department of Civil Engineering, University of Salerno, Via Giovanni Paolo II 132, 84084 Fisciano, SA, Italy
[b] Department of Structural Engineering, University of California, San Diego, CA, USA

ARTICLE INFO

Article history:
Received 8 August 2016
Received in revised form
6 October 2016
Accepted 12 October 2016
Available online 15 October 2016

Keywords:
Pentamode metamaterials
Large elastic strains
Seismic isolation
Impact protection

ABSTRACT

We study the mechanical response under large elastic strains of pentamode layers confined between stiffening plates, and the potential use of such systems as novel seismic isolation and impact protection devices. We analyze pentamode materials that exhibit three soft deformation modes in the infinitesimal stretching regime that follow by the presence of perfectly hinged connections between the rods. The response of these metamaterials under large elastic strains is characterized by an elastic-stiffening effect in terms of the lateral force-displacement response, which increases in the presence of rigid connections and decreases by increasing the number of layers. Our results lead us to conclude that the analyzed pentamode metamaterials can be effectively employed as novel, performance-based devices for seismic and mechanical vibration protection, by designing the lattice geometry, the stiffness properties of the joints, and the lamination scheme in a suitable manner and as a function of the operating conditions.

1. Introduction

In the last few years, mechanical and acoustic metamaterials have attracted the attention from different areas of research because of their unique behavior. Such smart materials are artificial structured lattices whose mechanical properties are mainly derived by their geometrical structure rather than their chemical composition (refer, e.g., to papers [1], [2]). The class of "extremal materials" has been introduced in Ref. [3] to define materials that behave as extremely stiff in some deformation modes while very soft in others. These are called uni-mode, bi-mode, tri-mode, quadra-mode and penta-mode materials, from the number of small deformation modes they can achieve. This definition applies to a special class of mechanical metamaterials - composite materials, structural foams, cellular materials, etc. - which feature special mechanical properties. A specific category of extremal materials, called pentamode metamaterials, have received particular attention in the literature. In particular, 3D printing techniques have been employed to manufacture such materials both at the macroscale [4], [5], and microscale [6].

Pentamode metamaterials have five very small eigenvalues, meaning that they are very soft in five out of six principal directions of the elasticity tensor. This means that they show a very large bulk modulus (B), as compared to their shear modulus (G). The properties peculiar to pentamode metamaterials lead them to be suitable for many applications, such as transformation acoustics and elasto-mechanical cloak (refer, e.g., to [7–10] and the references therein). Their potential in different engineering fields is still only partially explored.

One of the most promising application is the field of protection of structures from dynamic excitations either mechanically as well as naturally induced. For instance, while well established design and construction techniques exist to prevent the collapse of structures during seismic events, the requirement of limited damage was not often considered of paramount importance. Recently instead the structural engineering community recognized the importance to further investigate techniques that can reduce or even eliminate the damage that is typically sustained during these events (refer, e.g., to [11], [12], and the references therein). Under this perspective, the seismic isolation and energy dissipation technology, is receiving increased attention due to its effectiveness and ease of implementation on both existing and new structures. Seismic isolation is based on the fundamental concept of shifting the fundamental structural frequencies to ranges of reduced frequency content of the ground motion. This is commonly obtained with a significant increase of displacement capacity, often

* Corresponding author.
E-mail addresses: adaamendola1@unisa.it (A. Amendola), gbenzoni@ucsd.edu (G. Benzoni), f.fraternali@unisa.it (F. Fraternali).

http://dx.doi.org/10.1016/j.compositesb.2016.10.027
1359-8368/

associated with supplemental capacity of energy dissipation, introduced by ad-hoc designed devices. Among others, popular seismic isolators currently in use comprise elastomeric bearings, friction based bearings, and hybrid solutions [11–16].

The ability of pentamode lattices to have both very soft and very stiff deformation modes suggests they are potentially suitable for use as seismic isolators [5], [17–19]. Unlike most other seismic isolators, where the response depends entirely on the properties of the materials used, the response of pentamode lattices depends mostly on their geometry. This is advantageous, as their response can be easily tuned by altering the geometry to control the vertical and horizontal stiffness for each application [5]. Previous studies have investigated the bending-dominated response of confined pentamode structures formed by alternating lattices with a face-centered-cubic (fcc) unit cell and stiffening plates (*fcc systems*) [5], [17–19]. Here we study a different kind of metamaterials, which use pentamode lattices whose unit cell consists of one half of the fcc cell (*sfcc systems*, cf. Sect. 2). By simulating the mechanical response of physical models of sfcc systems in the large elastic strain regime, we observe a stiffening effect in terms of the lateral force vs. lateral displacement response with increasing amplitude of lateral displacements (Sect. 3). Such a geometrically nonlinear effect is accompanied by a softening response in vertical direction under mixed force-displacement loading, and becomes less effective by layering multiple sfcc layers, one over the other (cf. Sect. 3.2). It is worth noting that a similar hardening response is a desirable performance for seismic isolators potentially experiencing large displacements [20], [21]. Using a multi-layer design strategy, we are able to design laminated sfcc systems made of steel, which exhibit effective lateral stiffness comparable to that of a commercial seismic isolator made of soft rubber-pads and thin steel shims. In addition, the analyzed sfcc pentamode bearings are tension-capable, i.e., can bear both compression and tension vertical loads during seismic excitations, due to the nonzero tensile strength of the rods forming the pentamode lattices (refer, e.g., to the recent paper [22], and references therein, for the technical relevance of tension-capable bearings). Sect. 4 summarizes the main results of the present study and suggests future research lines aimed at exploring the engineering potential of the pentamode metamaterials.

2. Physical models of sfcc pentamode metamaterials

The present section numerically investigates the elastic response of physical models of laminated pentamode metamaterials that show elementary modules of four rods meeting at a point confined between stiffening plates (sfcc systems, see Fig. 1a). We employ steel bars grade S335JH, with Young modulus $E_o = 210$ GPa and yield strength $f_y = 355$ MPa [23], [24], which can be connected to each other through the ball joint systems typically used in space grids [25]. We analyze lattices with 2×2 sfcc unit cells on the horizontal plane, each composed of two elementary modules. The lattice constant a is set equal to 1200 mm, and the layer height is set equal to 600 mm. The stiffening plate edge length is equal to 2400 mm, and the rods are hollow circular tubes with length $\ell = 519.6$ mm.

We consider systems with hinged, rigid or semi-rigid connections, in order to account for technical difficulties related to the manufacturing process of perfectly hinged space grids. These problems are mainly due to the finite size of the bolts connecting the rods to the ball joints, and to friction effects at the nodes [25]. As we shall see, the analyzed systems may exhibit a marked stiffening response in the large elastic deformation regime (slope of the load-displacement curves markedly increasing with the lateral displacements). For that reason, and with the aim of preventing buckling and yielding effects during the service behavior, our first results refer to lattices equipped with thick rods that feature 76.1 mm diameter and 5 mm wall thickness ($s = 1{,}116.84$ mm^2) [23], which results in: $P_y = f_y\, s = 396.48$ kN. On assuming perfectly hinged connections, the Eulerian critical load of the generic rods is: $P_{cr} = \pi^2 E_o I/\ \ell^2 = 5444.23$ kN; $I = 709{,}220.30$ mm^4 denoting the moment of inertia of the cross-section. We will refer to such systems with the label 76SFCC. In Sect. 3.2, we will also examine lattices featuring relatively more slender rods, which have a 48.3 mm diameter and 5 mm wall thickness [23]; $s = 680.15$ mm^2; $I = 161{,}527.42$ mm^4; $P_y = 241.46$ kN; $P_{cr} = \pi^2 E_o I/\ \ell^2 = 1239.94$ kN. We will refer to systems equipped with such rods as 48SFCC systems hereafter.

3. Large elastic deformations

We study the response of the models illustrated in the previous section under large elastic strains. We examine a displacement loading condition, and a mixed, vertical force − lateral displacement loading condition on the top plate of the analyzed systems, always keeping the bottom plate at rest. The displacement loading condition is applied to a monolayer system, while the mixed loading condition is applied both to a monolayer and multilayer system.

Let F_x and F_z denote the total forces acting on the top plate of the current system in the x- and z- directions, respectively. We use solid lines to indicate branches of the force-displacement curves such that in all members it results $P < P_y$ (pre-axial-yielding branches: PAYB); and dashed lines to indicate branches in which it results $P \geq P_y$ in one or more rods. We omit the change in the rods' cross-sectional properties, due to transverse deformation effects, when performing the above axial yielding check (AYC). The study of the post-elastic behavior of the structures under examination is beyond the scope of the present work.

3.1. Displacement loading

We apply a two-step displacement loading history on the top plate of a monolayer 76SFCC system, on assuming quasi-static loading conditions. First, we apply a downward uniform vertical displacement $d_z = d_z^0 = -1.478$ mm to the top plate (vertical pre-loading). Next, we apply a uniform d_x- displacement ramp history to the top plate (in the positive $x-$ direction), by keeping the above d_z displacement fixed. The elastic response of the system under consideration is analyzed in the large displacement regime, through the commercial finite element software Sap2000® version 18 [26], [27], (Fig. 1), and an in-house discrete element code. We employ two different finite element models: one featuring semi-rigid connections between the beam elements that describe the

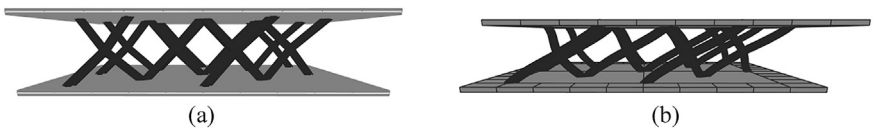

Fig. 1. Finite element model of a monolayer 76SFCC system under displacement loading: (a) reference configuration; (b) deformed shape under $d_x = 250$ mm (SRC-FEM).

rods (SRC-FEM); and the other exhibiting rigid connections between such elements (RC-FEM). The SRC-FEM is obtained by introducing partial fixity rotational springs at the ends of each rod, and prescribing the following stiffness coefficients (both in torsion and bending) to each

$$K_\vartheta = \alpha E_0 s \ell \tag{1}$$

where α denotes a dimensionless parameter, s denotes the cross-section area, ℓ denotes the rod length, and ϑ denotes the generic rotational degree of freedom (dof) at the end of the element [26]. Our simulation results assume $\alpha = 10^{-3}$, in order to allow the SRC-FEM to approximate a frame model with hinged/pinned connections. The RC-FEM instead assumes no releases of rotational dof at the extremities of each rod, and corresponds to prescribing $\alpha \to \infty$ in Eqn. (1). Finally, we employ a discrete element model (DEM) [28–29] that describes the junctions between the rods as point masses and the rods as linear springs, which implies a total release of the rotational dofs at the ends of each rod (perfectly hinged connections: $\alpha \to 0$). In each of the above models, we model the stiffening plates as rigid elements, both in-plane and out-of-plane (combined diaphragm and plates constraints [26]). The employed FEMs make use of the Nonlinear Static Analysis available in Sap2000®, taking into account both P-delta and large-displacement effects [26]. It is worth remarking that sfcc systems equipped with pin joints are unstable under incremental lateral displacements from the reference configuration [30]. For this reason, the response of the DEM equipped with hinged connections (HC-DEM) has been studied via the dynamic relaxation procedure presented in Ref. [31].

Table 1 shows the vertical stiffness coefficients $K_{v,0}$ recorded for the models under consideration in correspondence with the vertical preload phase (slope at the origin of the vertical force vs. vertical displacement curve). Such coefficients for the SRC-FEM and RC-FEM are similar to that of the HC-DEM, which shows the stretching-dominated character of the response of the current models. For all the such models, we estimate a vertical preload $F_z^0 \approx -1.8$ MN under the prescribed value of d_z^0, which corresponds to the vertical preload analyzed in the experimental tests on a commercial rubber bearing presented in Ref. [18–19] (the rubber bearing featured the following properties: diameter 0.85 m, height 0.35 m, 29 rubber layers of 7 mm each, 28 steel shims of 3.04 mm each, two terminal rubber layers of 31.8 mm each and covers, without lead plug data provided by Caltrans Testing Facility, University of California, San Diego).

Table 1
Vertical stiffness $\boldsymbol{K}_{v,0}$ [kN/mm] of the analyzed monolayer 76SFCC systems.

HC-FEM	SRC-FEM	RC-FEM
1.204E+03	1.207E+03	1.208E+03

Fig. 2 shows the force-displacement curves obtained for the HC-DEM, SRC-FEM and RC-FEM (see the inserts in Fig. 2 for the behavior near the origin of such models). The deformed shape of the SRC-FEM under $d_x = 250$ mm is graphically illustrated in Fig. 1b.

The results in Fig. 2 highlight a marked stiffening (or hardening) character of the F_x–d_x and F_z–d_x curves exhibited by the analyzed models, for large or moderately large values of d_x. In the small displacement regime, we instead note that the F_x–d_x curve of the HC-DEM features zero slope at the origin, which highlights that such a structure exhibits infinitesimal shear-type mechanisms from the reference configuration (cf. the insert in Fig. 2a). The F_x–d_x curve of the SRC-FEM instead shows a small positive slope at the origin. Finally, the F_x–d_x curve of the RC-FEM features a markedly positive slope for $d_x = 0$. All the F_z–d_x curves of the examined models start with $F_z \approx -1.8$ MN at $d_x = 0$, as a consequence of the vertical preload (see the insert in Fig. 2b). It is interesting to observe that the F_z force rapidly assumes positive values (tensile forces on the top plate), as the lateral displacement d_x grows, in the current loading conditions ($d_z = d_z^0 =$ const, while d_x grows). Of note here is that the analyzed systems are tension-capable [22], due to the nonzero tensile strength of the rods forming the pentamode lattices. The AYCs are violated already for $d_x \geq 10$ mm in the RC-FEM, as a consequence of the marked stiffening character of the force-displacement curve of such a system. The force-displacement curves of the SRC-FEM and HC-DEM are rather close together

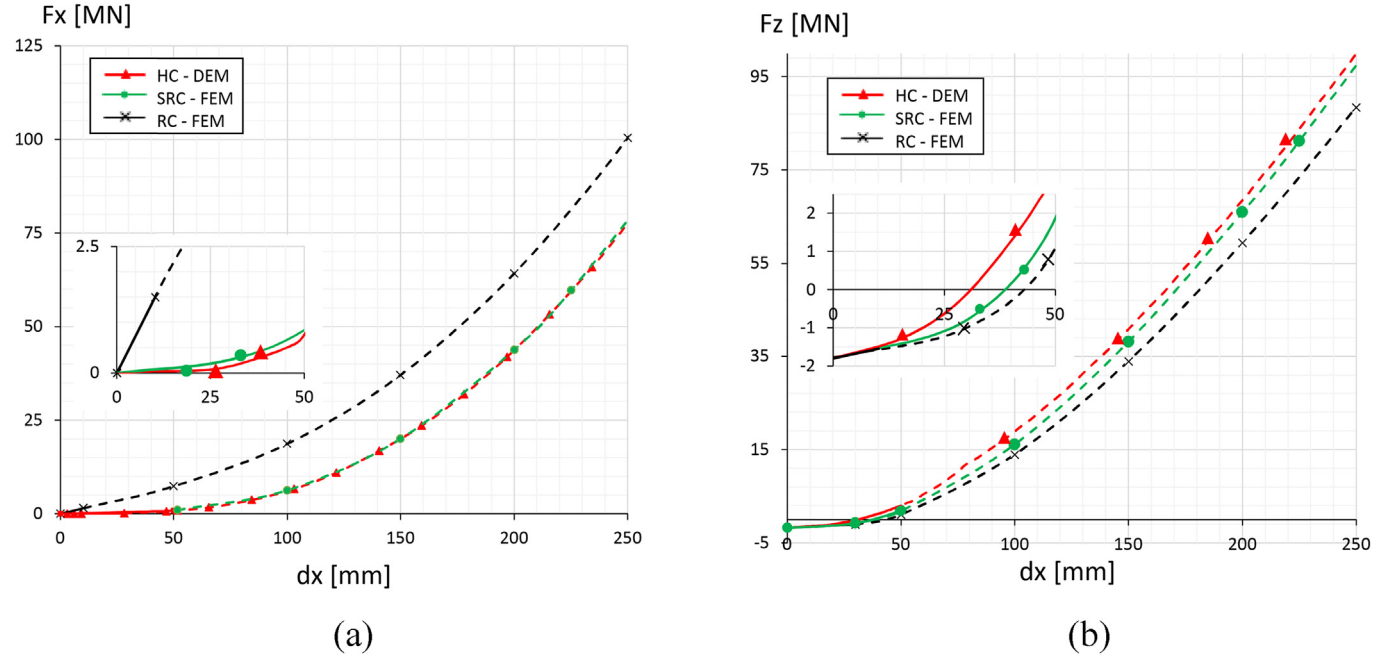

Fig. 2. Force vs. displacement curves of monolayer 76SFCC systems under displacement loading: (a) lateral force vs. lateral displacement; (b) vertical force vs. lateral displacement.

(stretching-dominated response), and the PAYBs of such curves extend up to $d_x \approx 50$ mm (Fig. 2). It is worth observing that, while the F_x–d_x curve of the RC-FEM is markedly stiffer than those of SRC-FEM and HC-DEM, the F_z–d_x curves of the SRC-FEM and HC-DEM have slightly greater slope than the F_z–d_x curve of the RC-FEM, (cf. Fig. 2 a and b).

3.2. Mixed force-displacement loading

Let us now study the response of a 76SFCC monolayer system under a fixed vertical load F_z, with increasing lateral displacements d_x of the top plate. We conduct such a study by focusing our attention on the SRC- and RC-FEMs described in the previous section, based on the consideration that perfectly hinged systems are not easily implemented in practice, especially when dealing with large displacements (due to unavoidable friction effects at the nodes). Fig. 3 shows the lateral force vs. lateral displacement curves obtained for the SRC-FEM and the RC-FEM in correspondence with several values of the vertical load F_z. The results in Fig. 3 highlight that the RC-FEM carries large horizontal forces and features a marked stiffening response under increasing lateral displacements, for any of the examined vertical loads, as we already observed under displacement loading conditions. The PAYB of such a system extends up to $d_x \approx 50$ mm under zero vertical load, and $d_x \approx 35$ mm under $F_z = -1.8$ MN. The F_x–d_x curves of the SRC-FEM instead feature a low-stiffness branch up $d_x \approx 400$ mm, which is followed by a markedly stiff branch ($d_x > 400$ mm). The PAYB of the SRC-FEM goes up to $d_x \approx 280$ mm under zero vertical load, and $d_x \approx 330$ mm under $F_z = -1.8$ MN.

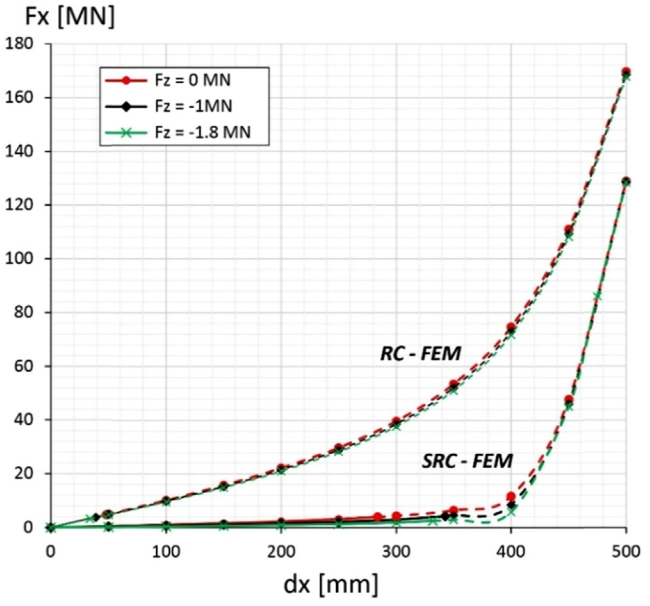

Fig. 3. Lateral force vs. lateral displacement curves of RC- and SRC-FEMs of monolayer 76SFCC systems under mixed force-displacement loading.

The multi-layer 76SFCC and 48SFCC systems were examined, under the same mixed loading condition as above, assuming $F_z = -1.0$ MN as vertical preload (Fig. 4). Table 2 shows the vertical stiffness coefficients $K_{v,0}$ obtained for the SRC-and RC-FEMs of such systems, which we will often denote by the short-hand notations SRC-76/48SFCC and RC-76/48SFCC, respectively. The $K_{v,0}$ coefficients of the models equipped with n_z layers are approximatively equal to $1/n_z$ of those competing to the corresponding monolayer systems.

The F_x–d_x curves of 76SFCC systems equipped with different numbers of layers are shown in Fig. 5. In the two- and three-layer systems equipped with semi-rigid connections, we observe a significant reduction of the hardening effect found in the monolayer case. The PAYB of the RC-76SFCC systems switches from $d_x < 39$ mm in the monolayer case to $d_x < 68$ mm and $d_x < 91$ mm in two- and three-layer systems, respectively. For the SRC-76SFCC systems, we observe that the PAYB of the monolayer case goes up to $d_x < 343$ mm, and that yielding does not occur at all in the two- and three-layer systems, up to $d_x = 500$ mm.

Table 3 compares the effective (secant) stiffness $K_{h,\text{eff}}$ of mono- and multi-layer systems at the end-points of the displacement ranges $d_x \in [0–250]$ mm and $d_x \in [0–500]$ mm. There is a marked abatement of $K_{h,\text{eff}}$ when passing from mono-to multi-layer systems. With reference to the loading interval $d_x \in [0–500]$ mm and the SRC-76SFCC models, we observe that the $K_{h,\text{eff}}$ of the systems with $n_z=2$ and $n_z=3$ are ~ 1/74 and ~ 1/133 of that exhibited by the monolayer system, respectively. In the same loading interval of the SRC-48SFCC models, the $K_{h,\text{eff}}$ of the systems with $n_z=2$ and $n_z=3$ are instead respectively ~ 1/68 and ~ 1/81 of the $K_{h,\text{eff}}$ corresponding to the case with $n_z=1$. It is worth noting that such reductions are much larger than the analogous reductions of $K_{v,0}$ when passing from mono-to multi-layer systems (cf. Tables 3 and 2).

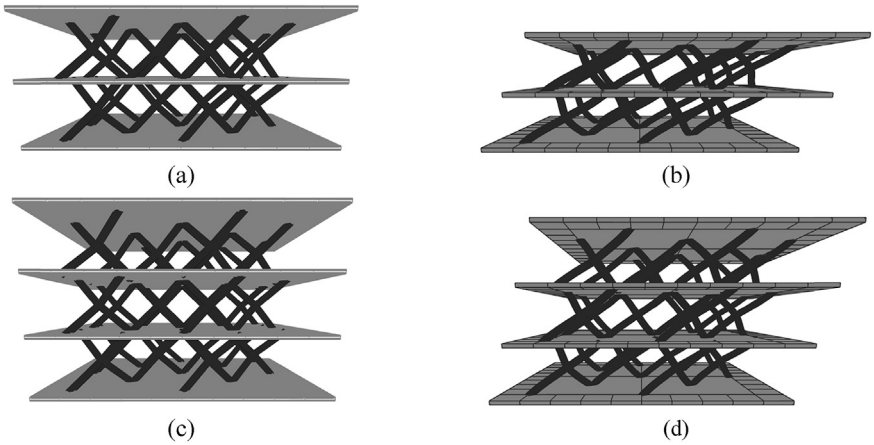

Fig. 4. Illustrations of multilayer SRC-76SFCC finite element models. (a–b): Reference configuration (a) and deformed shape under $d_x = 500$ mm (b) of a two-layer system. (c–d): Reference configuration (c) and deformed shape under $d_x = 500$ mm (d) of a three-layer system.

Table 2
Vertical stiffness $K_{v,0}$ [kN/mm] of the analyzed systems under mixed force-displacement loading, for varying numbers of layers n_z.

type	n_z	SRC-FEM	RC-FEM
76SFCC	1	1207.01	1208.04
76SFCC	2	610.70	621.10
76SFCC	3	417.52	420.50
48SFCC	1	736.55	747.60
48SFCC	2	368.14	373.66
48SFCC	3	245.27	248.95

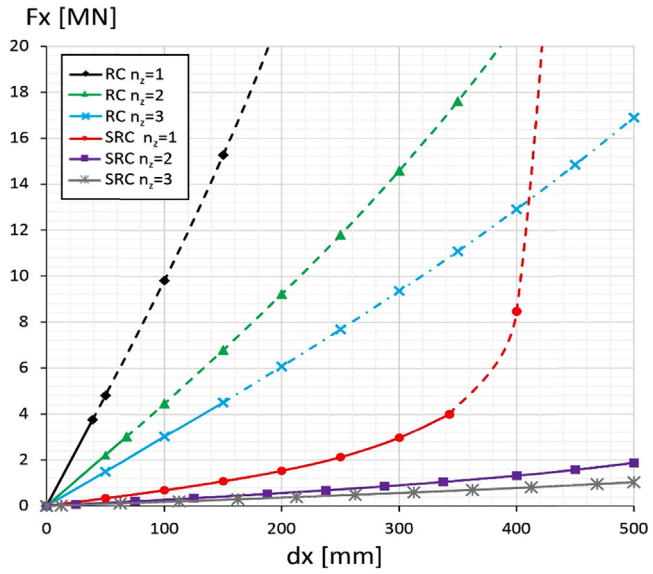

Fig. 5. Lateral force vs. lateral displacement curves of 76SFCC systems for varying numbers of layers n_z, under mixed force-displacement loading.

We also observe that the $K_{h,\text{eff}}$ exhibited at d_x= 500 mm by the SRC models are of the same order of magnitude of the $K_{h,\text{eff}}$ recorded for a commercial rubber bearing in Ref. [18–19] ($K_{h,\text{eff}}$~ 1.5–2.0 kN/mm; $K_{v,\text{eff}}$~ 700 kN/mm).

Fig. 6 (a) compares the lateral force vs. lateral displacement curves of SRC-76SFCC and SRC-48SFCC systems, and demonstrates that the PAYB of the monolayer 76SFCC system (d_x < 343 mm) is slightly wider than that of the monolayer 48SFCC system (d_x < 302 mm). The F_x vs. d_x curves of the 76SFCC systems are stiffer than those of the 48SFCC systems, in the cases with n_z = 1 and n_z= 2. In the three-layer case, 76SFCC and 48SFCC systems instead feature a similar F_x vs. d_x response, as confirmed by the results given in Fig. 6 (a) and Table 3. Fig. 6 (b) shows the vertical displacement vs. lateral displacement curves of the SRC-76SFCC systems with different numbers of layers (displacements of the top-most layer). Snapshots of the deformed configurations of single- and two-layer systems are provided in Fig. 7, in correspondence with selected values of the top-plate displacement d_x. The vertical displacements of the monolayer system are markedly larger than those exhibited by multilayer systems. The extremely large vertical displacements of the system with n_z = 1 would nearly reduce to zero the system height (d_z = 525 mm at d_x=500 mm, cf. panel (e) of Fig. 7). Such a vertical collapse event is associated with the extremely high stiffening character of the F_x–d_x response in Fig. 5 for d_x> 350 mm. It is worth noting, however, that the dashed branch of the d_z vs. d_x curve for n_z = 1 is just theoretical, since the monolayer 76SFCC system would actually experience plastic deformations for d_x > 343 mm, instead of a purely elastic response (post-buckling branch). As we already observed, the maximum vertical displacement markedly reduces in magnitude by increasing the number of layers.

Table 3
Effective horizontal stiffness $K_{h,\text{eff}}$ of the analyzed multilayer systems.

		RC–FEM		SRC - FEM	
		$K_{h,\text{eff}}$ [kN/mm]		$K_{h,\text{eff}}$ [kN/mm]	
type	n_z	[0–250] mm	[0–500] mm	[0–250] mm	[0–500] mm
76SFCC	1	115.97	337.15	8.49	257.24
76SFCC	2	47.20	57.83	2.88	3.74
76SFCC	3	30.72	33.78	1.85	2.07
48SFCC	1	26.81	182.65	5.21	167.95
48SFCC	2	10.35	13.74	1.76	2.47
48SFCC	3	6.77	7.62	1.86	2.07

We end by commenting on the distributions of the forces carried by the systems illustrated in Fig. 7. Our results indicate that the rods of both single- and two-layer systems carry almost uniform distributions of compressive axial forces in correspondence with the vertical preload phase (cf. panels (a)-(b) of Fig. 7). The compressive forces carried by the rods inclined towards the direction of the applied lateral displacement (i.e., towards the positive x-axis) progressively turn into tensile forces, for increasing values of d_x (see panels (c)-(f) of Fig. 7 for the deformed shapes corresponding to d_x > 0).

The configuration under d_x=500 mm of the single-layer system shows all the rods under tensile forces and the top plate almost collapsed onto the bottom plate. As we already noted, such a configuration is only theoretical, since it contemplates very large tensile forces in the rods inclined towards the positive x- axis, which are markedly greater than the yielding force P_y (cf. panel (i) of Fig. 7). Instead, the two-layer system carries much lower axial forces than the single-layer system. In such a system, tensile forces act in the rods inclined towards the +x- axis, and compressive forces act in the rods inclined towards the -x- axis. Both forces always result in P<P_y, up to d_x = 500 mm. With reference to such a system, we find that the shear forces carried by the rods grow with the lateral displacement d_x, featuring maximum values approximatively equal to 0.07, 0.19, 0.39, 0.54, 0.66 and 0.74 of the maximum axial forces, for d_x respectively equal to 50 mm, 100 mm, 200 mm, 300 mm, 400 mm and 500 mm. The bending moments approximately exhibit values equal in magnitude but opposite in sign at the ends of each rod, with extreme values circa equal to one half of the competent shear force multiplied by the rod length. Finally, the twisting moments carried by the rods are approximately one order of magnitude smaller than the bending moments. The above results provide evidence of a transition from a stretching-dominated response to a coupled stretching-bending regime of the systems equipped with semi-rigid connections, for growing values of the lateral displacements.

4. Concluding remarks

We have studied the nonlinear elastic response of novel metamaterials obtained by confining pentamode layers with stiff plates. We observed that the infinitesimal mechanisms exhibited by the examined systems in the small displacement regime switch to a stiffening lateral force vs. lateral displacement response under large displacements (Sect. 3). Such geometrically nonlinear behavior, which is also found in different lattice structures [32–34], can be finely adjusted by playing with the bending rigidity of the nodes and the number of layers (cf. Sect. 3.2).

The results of the present study allowed us to extend recent findings on the bending-dominated response of confined

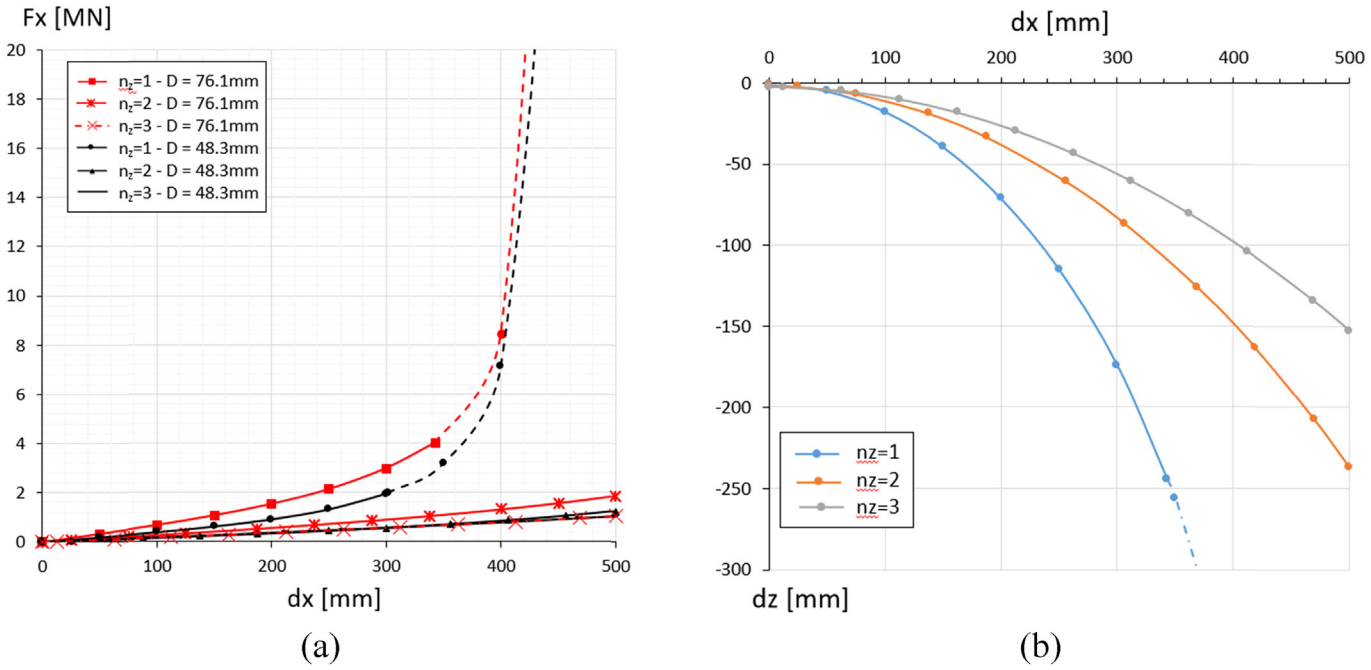

Fig. 6. (a) Lateral force vs. lateral displacement curves of SRC-76SFCC and SRC-48SFCC systems with different numbers of layers. (b) Vertical displacement vs. lateral displacement curves of 76SFCC systems showing different numbers of layers.

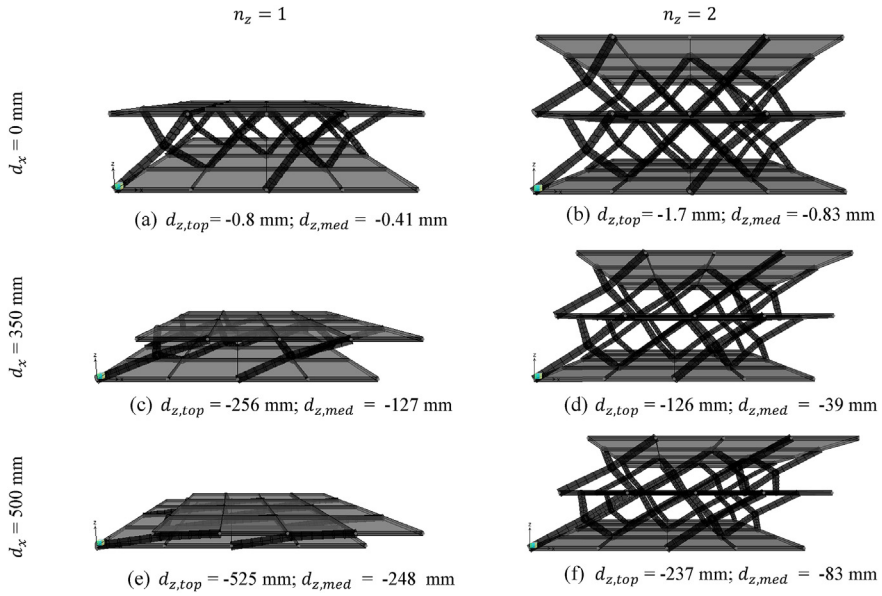

Fig. 7. Deformed configurations of SRC-FEMs relative to mono- and bi-layer 76SFCC systems, for different values of the top-plate lateral displacement d_x ($d_{z,top}$: vertical displacement of the top plate; $d_{z,med}$: vertical displacement of the mid-horizontal layer).

pentamode lattices [5], [17–19] to the case of the stretching-dominated or coupled stretching-bending response of sfcc pentamode metamaterials equipped with hinged or semi-rigid connections. We were able to design sfcc multi-layer systems entirely made of steel (using steel both for the stiffening plates and the pentamode lattices), which exhibit effective lateral stiffness approximatively equal to that of a commercial seismic isolator made of soft rubber-pads and thin steel shims (Sect. 3.2). Their use as stop-band materials for shear waves [7–9] within novel impact protection gears awaits attention.

We may conclude that pentamode bearings offer several advantages over other available structural bearings [11–14], which mainly follow from the fact that such systems can be easily designed to behave as tension-capable and performance-based systems, and because their mechanical properties are driven largely by the geometry of the lattice microstructure, rather than the chemical composition of the material (i.e, such systems behave as mechanical metamaterials). It is worth noting that it is possible to play with the lattice microstructure in order to achieve the desired combination of shear and compression response (cf. Sect. 3 and Refs. [5], [17–19]). Moreover, the choice of the material offers additional design opportunities, both in terms of the elastic

response, and for what concerns the energy dissipation properties of the system. We have also observed that it is possible to design laminated structures that feature multiple pentamode layers equipped with different materials and properties, while in laminated rubber bearings the only variable relative to the soft layers consists of the type of rubber [5]. Finally, pentamode bearings can be manufactured on employing rapid prototyping techniques that make use of single or multiple materials (metals, polymers, etc.) [4–6], and space grid technologies employing ball-joint systems [25].

Future extension of the present research will regard experimental testing of real-scale physical models of pentamode bearings [35], the modeling of plastic and fracture damage in the rods of pentamode bearings under significant strains [36–38], and discrete-to-continuum approaches to the mechanics of confined multilayered structures [39–41]. Peculiar features of the examined systems, which suggest additional directions for future work, include their increasing lateral rigidity and vertical deformability in the large lateral displacement regime (cf. Sect. 3.2). We recommend that future studies undertake detailed investigations of such geometrically nonlinear effects, with areas of focus including the examination of systems with variable numbers of layers, the inclusion of dissipative and stiffening members within the pentamode layers, and the use of lateral confinement/pre-stress techniques.

Acknowledgements

A. Amendola gratefully acknowledges financial support from the Ph.D. School in Civil Engineering at the University of Salerno. The authors wish to thank Gerardo Carpentieri from the Department of Civil Engineering of the University of Salerno, and Pasquale Gagliardi, from Vestrut Engineering s.r.l. (http://www.vestrut.it/en/), for their helpful assistance with the numerical results and the design of physical models of sfcc systems.

References

[1] Lu MH, Feng L, Chen YF. Phononic crystals and acoustic metamaterials. Mater. Today 2009;12:34–42.
[2] Maldovan M. Sound and heat revolution in phononics. Nature 2013;503:209–17.
[3] Milton GW, Cherkaev AV. Which elasticity tensors are realizable? J Eng Mater.-T 1995;117(4):483–93.
[4] Schittny M, Bückmann T, Kadic M, Wegener M. Elastic measurements on macroscopic three-dimensional pentamode metamaterials. Appl Phys Lett 2013;103.
[5] Amendola A, Smith CJ, Goodall R, Auricchio F, Feo L, Benzoni G, et al. Experimental response of additively manufactured metallic pentamode materials confined between stiffening plates. Compos Struct 2016;142:254–62.
[6] Kadic M, Bückmann T, Stenger N, Thiel M, Wegener M. On the practicability of pentamode mechanical metamaterials. Appl Phys Lett 2012;100.
[7] Martin A, Kadic M, Schittny R, Bückmann T, Wegener M. Phonon band structures of three-dimensional pentamode metamaterials. Phys Rev B 2010;86:155116.
[8] Huang Y, Lu X, Liang G, Xu Z. Pentamodal property and acoustic band gaps of pentamode metamaterials with different cross-section shapes. Phys Lett 2016;A 380(13):1334–8.
[9] Bückmann T, Thiel M, Kadic M, Schittny R, Wegener M. An elastomechanical unfeelability cloak made of pentamode metamaterials. Nat Comm 2014;5:4130.
[10] Chen Y, Liu X, Hu G. Latticed pentamode acoustic cloak. Sci Rep 2015;5:15745.
[11] Skinner RI, Robinson WH, Mcverry GH. An introduction to seismic isolation. Wiley; 1993.
[12] Kelly JM. Earthquake-resistant design with rubber. London: Springer-Verlag; 1993.
[13] Benzoni G, Casarotti C. Effects of Vertical Load, strain rate and cAYCling on the response of lead-rubber seismic isolators. J Earthq Eng 2009;13(3):293–312.
[14] Higashino M, Hamaguchi H, Minewaki S, Aizawa S. Basic characteristics and durability of low-friction sliding bearings for base isolation. Earthq Eng Eng Seismol 2003;4(1):95–105.
[15] Warn GP, Whittaker AS, Constantinou MC. Vertical stiffness of elastomeric and lead- rubber seismic isolation bearings. J Struct Eng.-ASCE 2007;133(9):1227–36.
[16] European Committee for Standardization. Anti-seismic devices, EN 15129. Brussels: Belgium; 2009.
[17] Amendola A, Carpentieri G, Feo L, Fraternali F. Bending dominated response of layered mechanical metamaterials alternating pentamode lattices and confinement plates. Compos Struct 2016;151:71–7.
[18] Fraternali F, Carpentieri G, Montuori R, Amendola A, Benzoni G. On the use of mechanical metamaterials for innovative seismic isolation systems. 2015. In: Compdyn 2015-5th Eccomas thematic conference on computational methods. In: Structural Dynamics and Earthquake Engineering, 349-358.
[19] Fabbrocino F, Amendola A, Benzoni G, Fraternali F. Seismic application of pentamode lattices. Ingegneria Sismica/International. J Earthq Eng 2016;1–2:62–71.
[20] Becker TC, Mahin SA. Experimental and analytical study of the bi-directional behavior of the triple friction pendulum isolator. Earthq Eng Struct Dyn 2012;41:355–73.
[21] Fenz DM, Constantinou MC. Modeling triple friction pendulum bearings for response-history analysis. Earthq Spectra 2008;24:1011–28.
[22] Zhou Z, Wong J, Mahin S. Potentiality of using vertical and three-dimensional isolation systems in nuclear structures. Nucl Eng Technol 2016;48(5):1237–51.
[23] EN 10210–2. Hot finished structural hollow sections of non-alloy and fine grain steels - Part 2: tolerances, dimensions and sectional properties. 2006.
[24] EN 1993-1-1:2005. Eurocode 3: design of steel structures - Part 1-1: General Rules and rules for buildings, european committee for standardization. May 2005.
[25] Chilton J. Space grid structures. UK: Oxford; 2000.
[26] CSI, Computers & Structures, Inc. Analysis reference manual for SAP2000® version 18. Berkeley, California, USA. June 2015.
[27] CSI, Computers & Structures, Inc. Steel frame design manual for SAP2000® version 18. Berkeley, California, USA. September 2015.
[28] Leonard A, Fraternali F, Daraio C. Directional wave propagation in a highly nonlinear square packing of spheres. Exp Mech 2013;53(3):327–37.
[29] Daraio C, Ngo D, Nesterenko VF, Fraternali F. Highly nonlinear pulse splitting and recombination in a two dimensional granular network. Phys Rev 2010;E 82:036603.
[30] Norris AN. Mechanics of elastic networks. Proc R Soc A 2014;470:20140522.
[31] Fraternali F, Blesgen T, Amendola A, Daraio C. Multiscale mass-spring models of carbon nanotube foams. J Mech Phys Solids 2011;59:89–102.
[32] Amendola A, Carpentieri G, De Oliveira M, Skelton RE, Fraternali F. Experimental investigation of the softening-stiffening response of tensegrity prisms under compressive loading. Compos Struct 2014;117:234–43.
[33] Fraternali F, Carpentieri G, Amendola A. On the mechanical modeling of the extreme softening/stiffening response of axially loaded tensegrity prisms. J Mech Phys Solids 2015;74:136–57.
[34] Fraternali F, Carpentieri G, Amendola A, Skelton RE, Nesterenko VF. Multiscale tunability of solitary wave dynamics in tensegrity metamaterials. Appl Phys Lett 2014;105:201903.
[35] Modano M, Fabbrocino F, Gesualdo A, Matrone G, Farina I, Fraternali F. On the forced vibration test by vibrodyne. 2015. COMPDYN 2015–5th ECCOMAS Thematic Conference on Computational Methods in Structural Dynamics and Earthquake Engineering, 209-217.
[36] Fraternali F. Free Discontinuity Finite element models in two-dimensions for in-plane crack problems. Theor Appl Fract Mec 2007;47:274–82.
[37] Schmidt B, Fraternali F, Ortiz M. Eigenfracture: an eigen deformation approach to variational fracture. Multiscale Model Sim 2009;7(3):1237–66.
[38] El Sayed T, Mock W, Mota A, Fraternali F, Ortiz M. Computational assessment of ballistic impact on a high strength structural steel/polyurea composite plate. Comput Mech 2009;43(4):525–34.
[39] Fraternali F, Lorenz CD, Marcelli G. On the estimation of the curvatures and bending rigidity of membrane networks via a local maximum-entropy approach. J Comput Phys 2012;231:528–40.
[40] Fraternali F, Marcelli G. A multiscale approach to the elastic moduli of biomembrane networks. Biomech Model Mechan 2012;11(7):1097–108.
[41] Schmidt B, Fraternali F. Universal formulae for the limiting elastic energy of membrane networks. J Mech Phys Solids 2012;60:172–80.